Journal of Environmental Statistics

September 2019, Volume 09, Issue 2. http://www.jenvstat.org

Area interaction point processes for bivariate point patterns in a Bayesian context

Glenna F. Nightingale [1], Janine B. Illian [2], Ruth King [3] and Peter Nightingale [4]

Glenna.Nightingale@ed.ac.uk, janine.illian@glasgow.ac.uk,
Ruth.King@ed.ac.uk, peter.nightingale@york.ac.uk,

[1]School of Health in Social Science, University of Edinburgh,
Edinburgh, EH1 2QL, U.K.

[2]School of Mathematics & Statistics, The Mathematics and Statistics Building,
University Place, Glasgow, G12 8QQ, U.K.

[3]School of Mathematics, University of Edinburgh,
James Clerk Maxwell Building, The Kings Buildings,
Peter Guthrie Tait Road, Edinburgh, EH9 3FD, U.K.

[4]Department of Computer Science, University of York, Deramore Lane, York, YO10 5GH U.K.

Abstract

In this paper we consider bivariate point patterns which may contain both attractive and inhibitive interactions. The two subpatterns may depend on each other with both intra- and interspecific interactions possible. We use area interaction point processes for quantifying both attractive and inhibitive interactions in contrast to pairwise interaction point processes, typically model regular point patterns. The ability to permit both attraction and repulsion is a valuable feature and allows for the modelling of different forms of interactions in a given community. The differentiation between intra- and interspecific interactions in one model accounts for the fact that the presence of a second species may "mask" or "magnify" existing intraspecific interactions. A Bayesian approach has been applied for estimating interaction parameters and for discriminating between eight competing research hypotheses. For the particular application to modelling the interactions of species in a highly biodiverse forest, this study reveals posterior support for an interspecific interaction of attraction between the two species considered and may serve to inform forest rehabilitation schemes relating to this forest. Overall, knowledge of the interactions of key species in any given forest would be invaluable to reforestation efforts if this forest is later ravaged by wildfires.

Keywords: area interaction, marked point patterns, Bayesian, point process, model uncertainty.

1. Introduction

The quantification of interspecies interactions is important for ecological studies, particularly those for which species coexistence (Turnbull, Levine, Loreau, and Hector 2013) is of primary interest. Interspecies interactions may assume one of three forms, attractive, inhibitive (repulsive) and neutral (no interaction). The area of interaction (or zone of influence) for a given plant denotes the zone around that plant within which it accesses vital resources (Casper, Schenk, and Jackson 2003). Plants which exhibit a highly regular spatial pattern are most likely to be repulsive to each other such that they inhibit sharing of resources (such as soil nutrients and sunlight) with another plant (due to competition) and thus inhibit coexistence in close proximity. Certain plants may appear to exist in close spatial proximity to other plants due to a symbiotic (Tedersoo 2017) relationship between these plants.

In this paper we model the species interactions in a data set consisting of observations of two plant species (a bivariate point pattern). It is important that the model adopted incorporates the zone of influence of the species under consideration. The area interaction point process is a useful choice to model a bivariate point pattern data set as it allows for the incorporation of the above-mentioned ecological concept of both attraction and repulsion.

2. Data

The statistical approach has been motivated by data from a highly diverse plant community (67 species, 6385 plants) in Western Australia (Illian, Møller, and Waagepetersen 2009). The two species are *Astroloma xerophyllum* ($n = 91$) and *Banksia menziesii* (n=25). Figure 1 shows the bivariate point pattern formed by the species pair. From the plot it is very difficult to visually detect any spatial correlation between the points representing the two species, however, the plot provides an indication (though not on an inferential level) of the position of the plants in relation to each other. Figure 2 shows plots of the univariate point patterns representing each species considered in the analyses. In addition, discs are drawn around each point of the pattern to denote the area of interaction (or zone of influence) associated with that plant. The interaction radius used for the discs for each species was calculated using biological information, specifically, the average circumference of the root network of the plants involved. This illustration provides a visual description of the degree of overlap between the zones of influence per univariate pattern. From these plots we can observe at a general level, that the degree of overlap of zones of influence is highest in the univariate point pattern for *A. xerophyllum*. The point pattern represented by the plant community from which the two species originate is depicted by Figure 3.

The species *Astroloma xerophyllum* is categorized as a *reseeder* whilst *Banksia menziesii* is categorized as a *resprouter* (Bell and Ojeda 1999). *Reseeders* respond to a fire stimulus by shedding seeds whereas the response of the *resprouters* is to regenerate from the remaining underground roots or tubers which were not destroyed by the fire (Atwell, Kriedemann, and Turnbull 1999; Kruger, Midgley, and Cowling 1997). We wish to investigate the intraspecific and interspecific interactions existing within the species pair. Biological literature suggests that there is a relationship of attraction between reseeders and reprouters (Bell and Pate 1996; Bell 2001; Read 1995), however the quantification of this interaction has not yet been done.

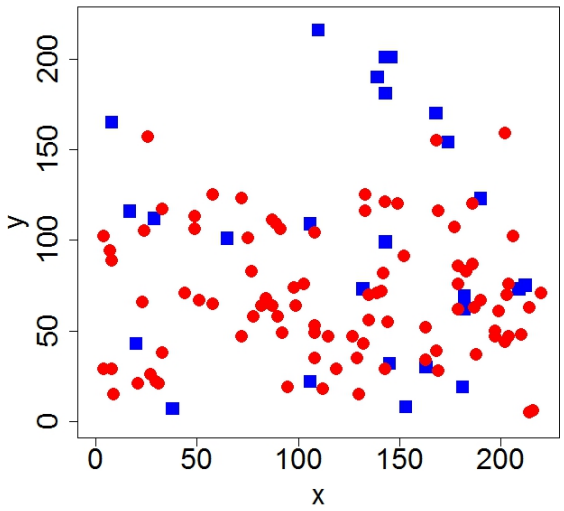

Figure 1: Plot showing the bivariate point pattern for the species pair comprising of *Astroloma xerophyllum* and *Banksia menziesii*. *Astroloma xerophyllum* is denoted by red filled circles. The sample area is 220 dm^2.

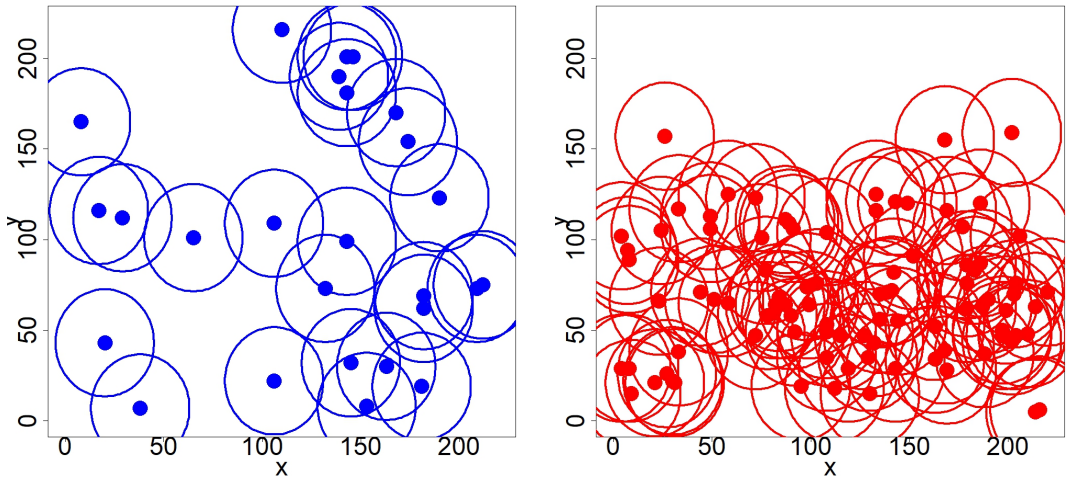

(a) (b)

Figure 2: Plots showing (a) the univariate point pattern for *B.menziesii*, and (b) the univariate point pattern for *A.xerophyllum*. The points in each plot are superimposed by the corresponding discs centered at that point. Each point pattern represents data taken from a forest of area 220 dm^2.

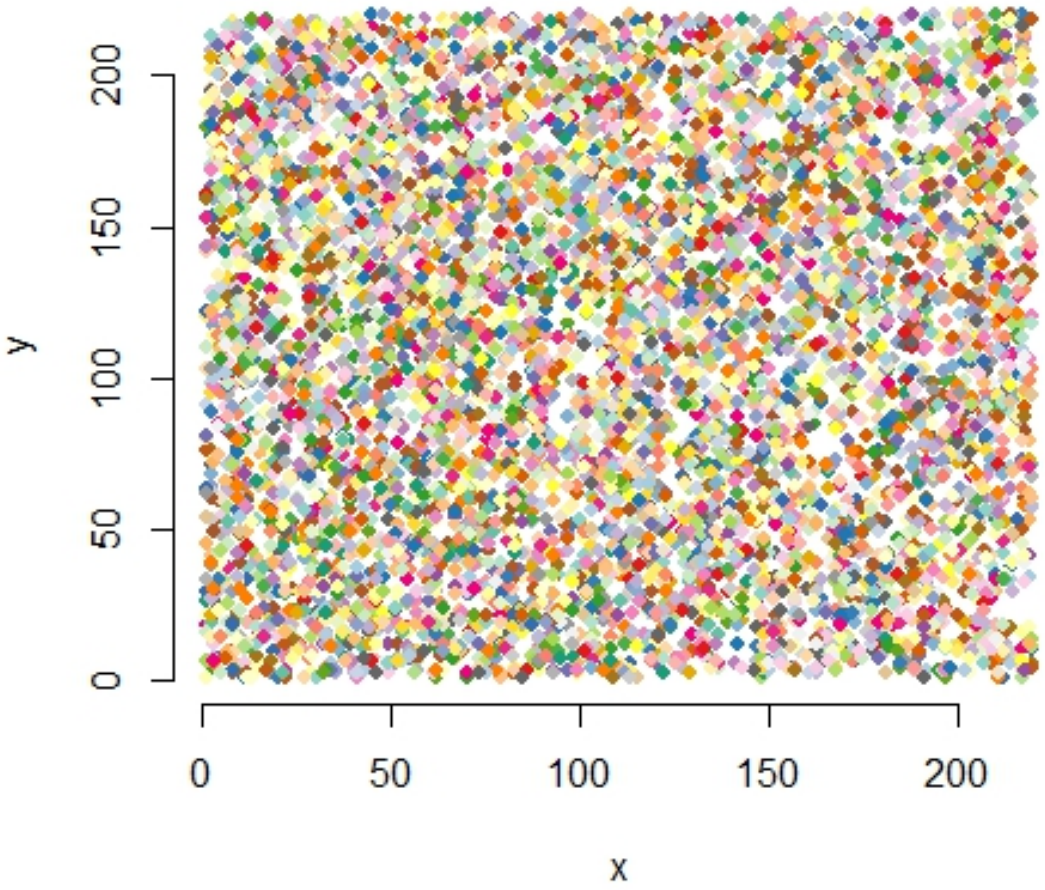

Figure 3: Point pattern which represents the entire plant community from which the two species under consideration originate.

3. Exploratory analysis

We now discuss the exploratory analysis of the bivariate point pattern of the species pair to obtain some preliminary insight on the structure of the pattern.

We employ the pair correlation function to analyse the second order behaviour of the pattern in each of the univariate patterns, see Figure 4. These functions are commonly used in summarizing point patterns (Stoyan and Stoyan 1996). The pair correlation functions for the univariate point pattern of each species are shown in Figure 4. For *Astroloma xerophyllum*, the plot of the pair correlation function in Figure 4(a) shows the graph (solid line) generally above (outside) the simulated envelope of the Poisson process reference line including at

the interaction radius of 25 dm (determined from biological characteristics of this species). In addition, the estimated function lies predominantly above (outside) of the simulation envelope generated from 1000 realizations of a bivariate homogeneous Poisson process. This suggests that the point pattern may be clustered. This is also supported by the plot of the K-function for this pattern in Figure 4(c). The associated K-function lies consistently above and outside of the simulation envelope generated from 1000 realizations of a univariate homogeneous Poisson process. Overall, neither the pair correlation function nor the K-function converge for *Astroloma xerophyllum*, which means that there might be some inhomogeneity in the pattern as well as clustering and the relative scales of these two processes is hard to distinguish, given the small number of points.

In contrast, for *Banksia menziesii*, the graph of the pair correlation function depicted in Figure 4(b), generally lies close to the Poisson reference line and within the simulation envelope for all the values shown in Figure 4(b). Similarly, the K-function (Figure 4(d)), suggests little clustering or regularity in the pattern. Care needs to be taken in interpreting these plots since the species are considered individually, thus ignoring other possible interactions.

The cross pair correlation function was used to analyze the bivariate point pattern and to detect any spatial dependence between the two species. The cross pair correlation function measures the spatial dependence (or spatial proximity) between marks within a multitype point pattern. Figure 5 shows the plot of the cross pair correlation function for the bivariate point pattern. The plot lies predominantly on the dotted reference line (which represents lack of spatial dependence/correlation), thus providing no evidence of interaction between the two species. As above, care needs to be taken when interpreting such preliminary analyses. The cross pair correlation function only uses interpoint distances (as opposed to area interaction calculations) to infer spatial dependence. In addition, there are few points in the patterns and hence estimation is hard - and simulation envelopes will be wide.

The initial exploratory analyses suggest that at the interaction radius of 25 dm there may be an attractive intraspecific interaction between plants of the species *Astroloma xerophyllum* but little evidence for the presence of an intraspecific interaction between plants of *Banksia menziesii*. Note that these analyses are based on the separate univariate patterns which are sub-patterns of the bivariate pattern formed by the locations of the two species. The presence of a second species or multiple species may affect the intraspecific interactions associated with each species; either 'masking' the presence of an intraspecific interaction or magnifying existing intraspecific interactions. The presence of another species adds to the complexity of the interactions involved and in fact, the various factors which affect the interactions of any given species in an ecological community may oppose or reinforce each other (Levine 2000).

The exploratory analysis for this species pair suggests that the point pattern representing *Astroloma xerophyllum* is clustered (with some inhomogeneity) and that of *Banksia attenuata* is random. In addition, based on ecological information (Bell 2001) we suspect that there is more going on (such as a specific ecological association between the two species) than just one clustered and one 'random' pattern - and that by considering more complex models we can reveal whether this is likely to be the case. We therefore choose instead to adopt a bivariate area interaction process to model this species pair. In particular, with this model we can simultaneously assess intra- and interspecific interactions - and use appropriate model selection to qualitatively compare competing biological hypotheses.

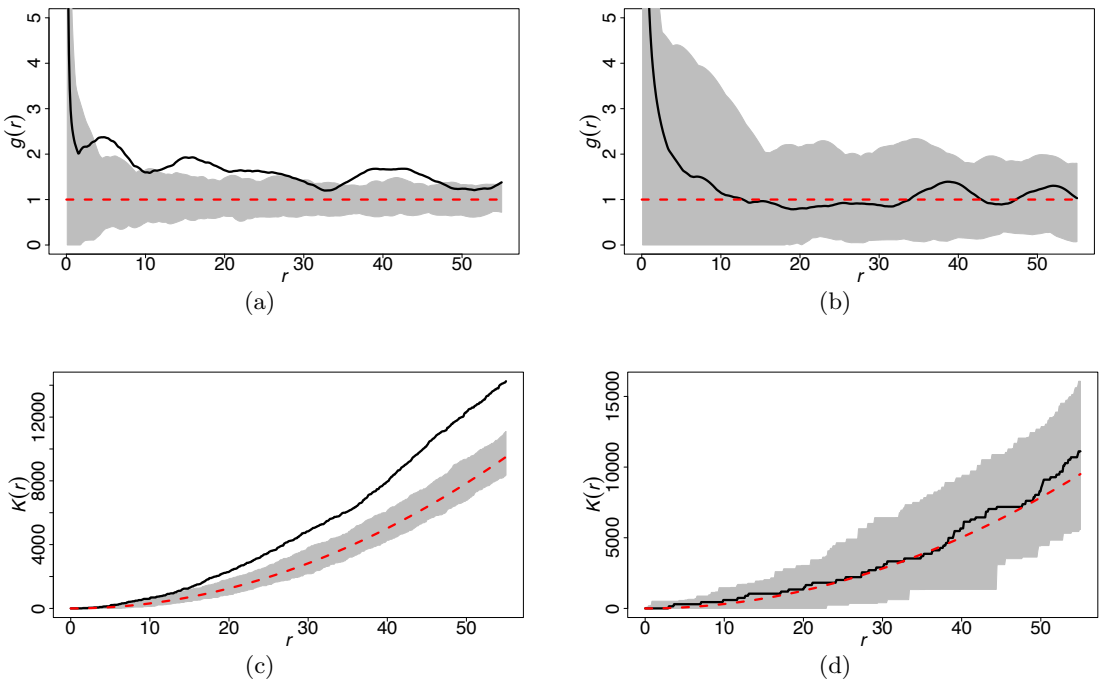

Figure 4: Plots (a) and (b) show the pair correlation analyses for *Astroloma xerophyllum*, and *Banksia menziesii*, respectively. The solid line represents the plot of the pair correlation function at each distance and the dotted line represents the theoretical value for the pair correlation under a Poisson model where the interaction is constant at 1 for complete spatial randomness (CSR). Plots (c) and (d) show the plots of Ripley's K-function for each species where the solid line represents the function plotted using the data and the dotted line represents the theoretical plot for simulated data realized from a homogeneous Poisson process. The x axis for each plot represents the distance in decimeters. Envelopes (using 1000 simulations from a homogeneous Poisson process) are provided for each plot.

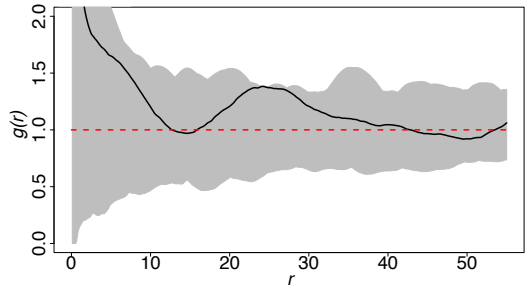

Figure 5: Plot showing the cross pair correlation function for the bivariate pattern formed by the species pair with a simulation envelope derived from 1000 realizations of a bivariate homogeneous Poisson process. The x axis represents the distance in decimeters.

4. Pairwise and Area interaction processes

We aim to use a model that allows for both attractive and inhibitive interactions among points. For this reason we consider an area interaction process, also known as the Widom-Rowlinson 'penetrable sphere mode' of liquid-vapour equilibrium (Baddeley and Turner 2000). Pairwise interaction processes model interactions within and between species. The interactions are quantified on a scale of 0 to 1 where lower values represent stronger levels of inhibition. However, pairwise point processes are generally used to model inhibitory interactions whilst area interaction processes model both inhibition and attraction. The fundamental difference therefore, between pairwise and area interaction processes lies in the specification of the interaction function for each process. For pairwise interaction processes, the interaction function is expressed as a function of the Euclidean distance between each pair of points in the pattern. In contrast, the interaction function of an area interaction process is expressed as the area of the union of discs associated with each point in the point pattern. We specify the radius of the discs as being equal to the specified interaction radius of the process. For modelling both attractive and inhibitory interactions we consider area interaction processes. We specify an interaction radius of 25 dm for each species. The specification of the interaction radius is based on the interaction radius range described by Illian *et al.* (2009) for *Banksia menziesii* and *Astroloma xerophyllum*.

In other studies where point processes are used and the specification of an interaction radius is required, the interaction radius is derived from biological knowledge (Nightingale, Illian, and King 2015; King, Illian, King, Nightingale, and Hendrichsen 2012; Illian and Hendrichsen 2010) and visual inspection of exploratory plots such as the plot of Ripley's K-function (Picard, Bar-Hen, Mortier, and Chadœuf 2009). The interaction radius may also be more formally estimated by using a profile likelihood approach (Illian and Hendrichsen 2010; Møller and Waagepetersen 2003; King *et al.* 2012).

We consider a bivariate area interaction point process that may be used to model both clustered and regular point patterns (Picard *et al.* 2009; van Lieshout 2000; Baddeley and Turner 2000; Baddeley and Lieshout 1995). Recall that a bivariate point pattern is a marked point pattern containing marks with two levels.

4.1. Mathematical notation

For a bivariate point pattern (see Figure 6), let the two species be denoted species 1 and species 2. The intensity parameters for the area interaction point process are denoted by β_1 and β_2 which represent the intensity for species 1 and species 2, respectively. The interaction parameters are γ_{11}, γ_{22}, γ_{12} and γ_{21} which denote the intraspecific interaction within species 1, the intraspecific interaction within species 2, the effect of species 1 on species 2, and the effect of species 2 on species 1, respectively. The parameter set is $\boldsymbol{\theta} = \{\beta_1, \beta_2, \gamma_{11}, \gamma_{22}, \gamma_{12}, \gamma_{21}\}$. We consider a symmetric area interaction point process, so that we set $\gamma_{12} = \gamma_{21}$ to avoid the terms being confounded. The full parameter set for this model becomes $\boldsymbol{\theta} = \{\beta_1, \beta_2, \gamma_{11}, \gamma_{22}, \gamma_{12}\}$. Note that for the area interaction point process, $\gamma_{ij} \geq 0 \quad \forall i, j$. Values lower than 1 represent inhibition; values greater than 1 represent attraction; and a value of 1 corresponds to no interaction.

Probability density function

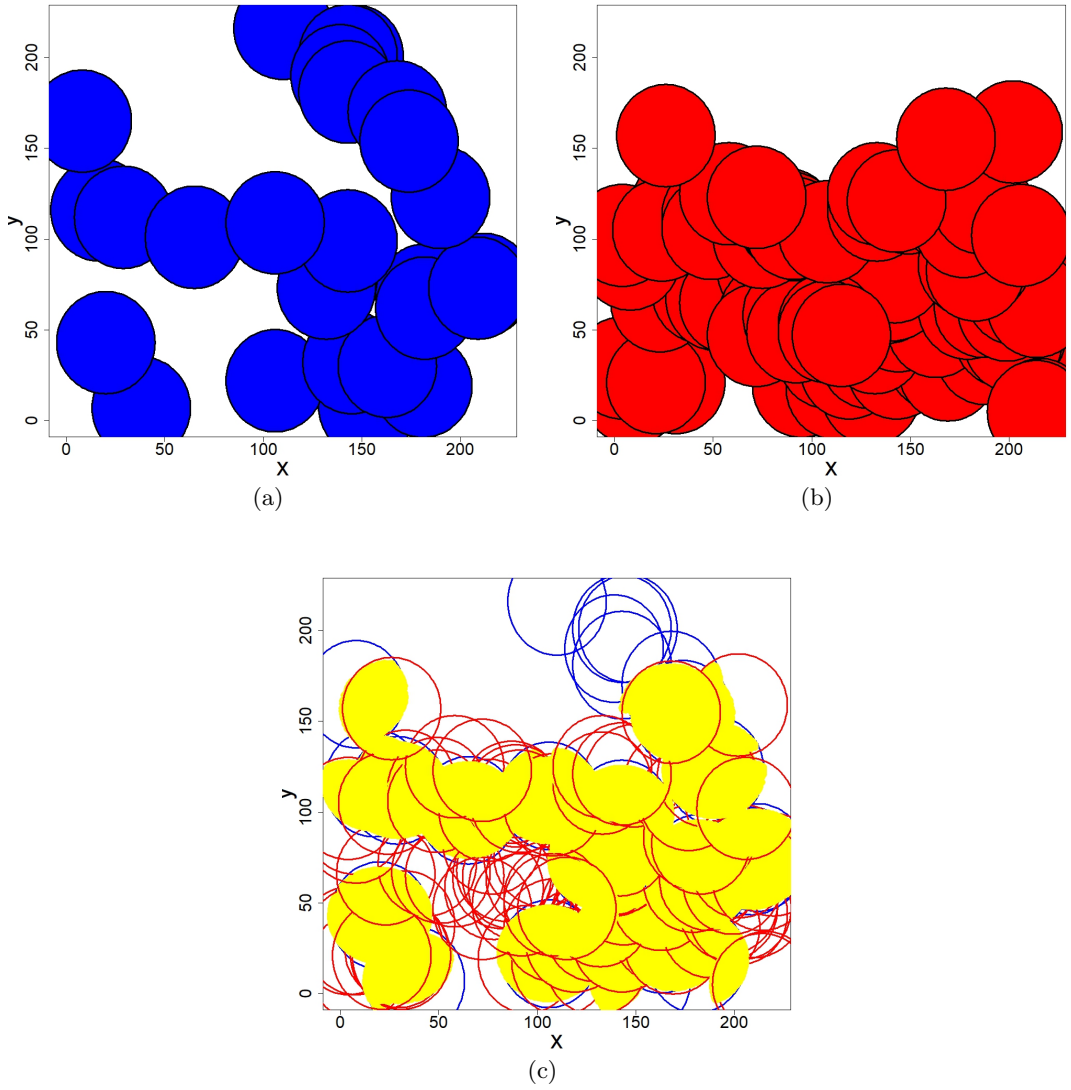

Figure 6: Illustration of the (a) area of the union of the discs representing *Astroloma xerophyllum*, the (b) area of the union of the discs representing *Banksia menziesii*, and (c) the area of intersection between the two species.

The density function for an area interaction process in a region of space W (Picard *et al.* 2009; Baddeley and Turner 2000; van Lieshout 2000; Baddeley and Lieshout 1995) can be generally defined in the form:

$$f(\boldsymbol{x}) \propto \beta^{n(\boldsymbol{x})}\gamma^{-|U_{\boldsymbol{x},r}|}, \tag{1}$$

where $n(x)$, β and γ are the total number of points, the intensity and interaction parameters respectively. The observed bivariate point pattern is denoted by $\boldsymbol{x}$ and the component univariate point patterns are denoted by $\boldsymbol{x_1}$ (species 1) and $\boldsymbol{x_2}$ (species 2) respectively. Note that the interaction radius is denoted as r. The term $|U_{\boldsymbol{x},r}|$ is expressed as

$$|U_{\boldsymbol{x},r}| = \bigcup_{i=1}^{n} B(x_i, r), \tag{2}$$

where $B(x_i, r)$ is a disc of radius r centered at each data point x_i (Baddeley and Lieshout 1995) such that

$$B(x_i, r) = \left\{a \in \Re^2 : \|a - x_i\| \leq r\right\}.$$

Analytically, the term $|U_{\boldsymbol{x},r}|$ is the union of the area of the discs of radius r centred at x_i (Baddeley and Lieshout 1995; Baddeley and Turner 2000; Picard *et al.* 2009).

The area of the union of discs may be expressed as the decomposition of the union of grains, $|U_{\boldsymbol{x},r}|$, in an inclusion-exclusion style (Picard *et al.* 2009; van Lieshout 2000). This is expressed concisely as:

$$|U_{\boldsymbol{x},r}| = \sum_{i=1}^{n(\boldsymbol{x})} |B(x_i, r)| - \sum_{i<j} |B(x_i, r) \cap B(x_j, r)| + ... + (-1)^{n(\boldsymbol{x})+1} \left| \bigcap_{i=1}^{n(\boldsymbol{x})} B(x_i, r) \right|. \tag{3}$$

The area of the union of discs is related to the interaction parameters of the area interaction point process (van Lieshout 2000, 2006). In the case of the bivariate pattern, this area can be decomposed into the area of the union of discs representing species 1 (Ξ) as shown in Figure 6(a), the area of the union of discs representing species 2 (Δ) as shown in Figure 6(b), and the area of intersection between Ξ and Δ as shown in Figure 6(c). This decomposition of the area of the union of the discs allows for the marks to be related to the interactions γ_{11}, γ_{22}, and γ_{12} as discussed by Picard *et al.* (2009).

Recall the expression for the decomposition of the area of the union of discs (following Möbius' inclusion-exclusion theorem) in Equation (3). Based on this expression we write the likelihood for the bivariate area interaction point process in an inclusion-exclusion style thus allowing for the marks ($m \in \{1, 2\}$) to be related to the interactions (Picard *et al.* 2009). The density function is given by:

$$f(\boldsymbol{x}) \propto \prod_{m=1}^{M} \beta_m^{n(\boldsymbol{x})} \gamma_{mm}^{-|U_{x_m, r_m}|} \prod_{m<m'} \gamma_{mm'}^{|U_{x_m, r_{mm'}} \cap U_{x_{m'}, r_{mm'}}|}. \tag{4}$$

For $m = 2$, this expression becomes

$$f(\boldsymbol{x}) \propto \beta_1^{n_1} \beta_2^{n_2} \gamma_{11}^{-|U_{x_1, r_1}|} \gamma_{22}^{-|U_{x_2, r_2}|} \gamma_{12}^{|U_{x_1, r_{12}} \cap U_{x_2, r_{12}}|}, \tag{5}$$

where n_1, n_2 denote the number of points representing species 1 and species 2, x_m, the point pattern representing species m where $m \in \{1, 2\}$, r_m and $r_{mm'}$, the specified interaction radius

for the interaction between individuals of species m and between species m and m' and $\gamma_{mm'}$, the interaction between individuals of species m and m' respectively.

Note that in this data set, $r_1 = r_2 = r_{12} = 25dm$ represent the interaction radii associated with intraspecific interactions related to species 1, intraspecific interactions related to species 2 and the interaction between the two species respectively. For simplicity, we express the density function for a bivariate area interaction process as:

$$f(\boldsymbol{x}) \propto \beta_1^{n_1}\beta_2^{n_2}\gamma_{11}^{-A_1(\boldsymbol{x})}\gamma_{22}^{-A_2(\boldsymbol{x})}\gamma_{12}^{A_{12}(\boldsymbol{x})}$$

where $A_1(\boldsymbol{x})$, $A_2(\boldsymbol{x})$ and $A_{12}(\boldsymbol{x})$ denote the area of the union of discs centered at the points in $\boldsymbol{x_1}$, the area of the union of discs centered at $\boldsymbol{x_2}$, and the area of intersection of $A_1(\boldsymbol{x})$ and $A_2(\boldsymbol{x})$ respectively. In other words, the areas $A_1(\boldsymbol{x}) = |U_{x_1,r_1}|$, $A_2(\boldsymbol{x}) = |U_{x_2,r_2}|$, and $A_{12}(\boldsymbol{x}) = |U_{x_1,r_{12}} \cap U_{x_2,r_{12}}|$. These areas are illustrated in Figures 6(a), 6(b) and 6(c) respectively.

Note that $f(\boldsymbol{x})$ is only known up to proportionality with the normalization constant analytically intractable. Thus, we consider the pseudolikelihood which is discussed in the following section.

Conditional intensity and pseudolikelihood

For a point ξ in $\boldsymbol{x}_1$, in a bounded region W, the conditional intensity is written as:

$$\begin{aligned}\lambda(\xi;\boldsymbol{x}_1) = \frac{f(\boldsymbol{x})}{f(\boldsymbol{x}\backslash\xi)} &= \frac{\beta_1^{n_1}\beta_2^{n_2}\gamma_{11}^{-A_1(\boldsymbol{x})}\gamma_{22}^{-A_2(\boldsymbol{x})}\gamma_{12}^{A_{12}(\boldsymbol{x})}}{\beta_1^{n_1-1}\beta_2^{n_2}\gamma_1^{-A_1(\boldsymbol{x}\backslash\xi)}\gamma_{22}^{-A_2(\boldsymbol{x}\backslash\xi)}\gamma_{12}^{A_{12}(\boldsymbol{x}\backslash\xi)}} \\ &= \beta_1\gamma_{11}^{-A_1(\xi)}\gamma_{12}^{A_{12}(\xi)}.\end{aligned}$$

For $\xi \in \boldsymbol{x_2}$, the conditional intensity becomes

$$\lambda(\xi;\boldsymbol{x_2}) = \beta_2\gamma_{22}^{-A_2(\xi)}\gamma_{12}^{A_{12}(\xi)}$$

since $\gamma_{12} = \gamma_{21}$ and $A_{12}(\xi) = A_{21}(\xi)$. We now consider the conditional intensity of a point $u_m \notin \boldsymbol{x}$ using the example of $u_1 \notin \boldsymbol{x}$. For a point $u_1 \notin \boldsymbol{x}$, the conditional intensity can be expressed as:

$$\begin{aligned}\lambda(u_1;\boldsymbol{x}) = \frac{f(\boldsymbol{x}\cup\{u_1\})}{f(\boldsymbol{x})} &= \frac{\alpha\beta_1^{n_1+1}\beta_2^{n_2}\gamma_{11}^{-A_1(\boldsymbol{x}\cup\{u_1\})}\gamma_{22}^{-A_2(\boldsymbol{x})}\gamma_{12}^{A_{12}(\boldsymbol{x}\cup\{u_1\})}}{\alpha\beta_1^{n_1}\beta_2^{n_2}\gamma_{11}^{-A_1(\boldsymbol{x})}\gamma_{22}^{-A_2(\mathbf{x})}\gamma_{12}^{A_{12}(\boldsymbol{x})}} \\ &= \beta_1\gamma_{11}^{-A_1(u_1)}\gamma_{12}^{A_{12}(u_1)},\end{aligned}$$

where $A_1(u_1)$ denotes the additional area (area of non overlap or *single* occupancy) contributed by the point u_1, to $A_1(\boldsymbol{x})$. This is essentially the difference in area between $A_1(\boldsymbol{x})$ and $A_1(\boldsymbol{x}\cup\{u_1\})$. The term $A_{12}(u_1)$ denotes the area of *double* occupancy with respect to $\boldsymbol{x_1}$ and $\boldsymbol{x_2}$, contributed by the point u_1.

The pseudolikelihood $PL(\boldsymbol{\theta};\boldsymbol{x})$, is the product of conditional intensities (Baddeley and Turner 2000) for each point in the data set and the exponential integrals that replace the previous intractable normalising constant. Note that $\gamma_{12} = \gamma_{21}$, but we initially retain the notation γ_{12} and γ_{21} for mathematical simplicity. Thus we have that:

$$PL(\boldsymbol{\theta};\boldsymbol{x}) = \prod_{j=1}^{n_2}\prod_{i=1}^{n_1}\beta_1\beta_2\gamma_{11}^{-A_1(\xi_i)}\gamma_{22}^{-A_2(\xi_j)}\gamma_{12}^{A_{12}(\xi_i)}\gamma_{21}^{A_{21}(\xi_j)}$$

$$\times \exp\left(-\beta_1 \int_W \gamma_{11}^{-A_1(u_1)} \gamma_{12}^{A_{12}(u_1)}\right) \exp\left(-\beta_2 \int_W \gamma_{22}^{-A_2(u_2)} \gamma_{21}^{A_{21}(u_2)}\right) \quad \forall u \in W$$

$$= \beta_1^{n_1} \beta_2^{n_2} \gamma_{11}^{-\sum_{i=1}^{n_1} A_1(\xi_i)} \gamma_{22}^{-\sum_{j=1}^{n_2} A_2(\xi_j)} \gamma_{12}^{2\sum_{i=1}^{n_1} A_{12}(\xi_i)}$$

$$\times \exp\left(-\beta_1 \int_W \gamma_{11}^{-A_1(u_1)} \gamma_{12}^{A_{12}(u_1)}\right) \exp\left(-\beta_2 \int_W \gamma_{22}^{-A_2(u_2)} \gamma_{12}^{A_{12}(u_1)}\right)$$

since $A_{12}(\xi_i) \equiv A_{21}(\xi_j)$ and $\gamma_{12} \equiv \gamma_{21}$.

This expression for the pseudolikelihood can be recast with the following notation for ease of interpretation and discussion:

$$PL(\boldsymbol{\theta}; \boldsymbol{x}) = \beta_1^{n_1} \beta_2^{n_2} \gamma_{11}^{-\psi_1(\boldsymbol{x_1})} \gamma_{22}^{-\psi_2(\boldsymbol{x_2})} \gamma_{12}^{2\psi_{12}(\boldsymbol{x})}$$

$$\times \exp\left(-\beta_1 \int_W \gamma_{11}^{-\psi_1^*(u_1)} \gamma_{12}^{\psi_{12}^*(u_1)}\right) \exp\left(-\beta_2 \int_W \gamma_{22}^{-\psi_2^*(u_2)} \gamma_{12}^{\psi_{12}^*(u_1)}\right) \tag{6}$$

where $\psi_1^*(u_1)$ represents the additional area (*single* occupancy area) incurred to the union of discs centered at points in $\boldsymbol{x_1}$ by the addition of the point u_1. The term $\psi_{12}^*(u_1)$ represents the additional area of intersection between discs (double occupancy area) centered at points in $\boldsymbol{x_1}$ and $\boldsymbol{x_2}$ incurred when a point u_1 is added to the data $\boldsymbol{x_1}$. Recall that $\psi_1(\boldsymbol{x_1})$ represents the sum of the *single* occupancy area associated with each point in the data set $\boldsymbol{x_1}$.

The analyses are run using the pseudolikelihood in the standard form transformed into the canonical form for of ease of interpretation. In the canonical form, the intensity parameter κ and the interaction parameter η are related to that of the standard form such that $\beta = \kappa\eta$ and $\gamma = \eta^{\frac{1}{\pi r^2}}$. The full parameter set for the canonical form is $\boldsymbol{\theta} = \{\kappa_1, \kappa_2, \eta_{11}, \eta_{22}, \eta_{12}\}$.

We now transform the variables in the pseudolikelihood in Equation (6) to obtain the canonical form. The corresponding pseudolikelihood is:

$$PL(\boldsymbol{\theta}; \boldsymbol{x}) = \alpha(\boldsymbol{\theta}) \kappa_1^{n_1} \kappa_2^{n_2} \eta_{11}^{n_1 - \frac{1}{\pi r^2}(\psi_1(\boldsymbol{x_1}))} \eta_{22}^{n_2 - \frac{1}{\pi r^2} - (\psi_2(\boldsymbol{x_2}))} \eta_{12}^{\frac{2}{\pi r^2}\psi_{12}(\boldsymbol{x})} \tag{7}$$

where $\alpha(\boldsymbol{\theta})$ is a function of parameters and is denoted by the exponentiated integral terms as shown in Equation 6. The integrals (intractable due to the multi-dimensionality) are estimated using a two-dimensional numerical integration approach of Simpson's rule routine for calculating the double integrals .

In this paper we refer to *Astroloma xerophyllum* as species 1 and *Banksia menziesii* as species 2 and consider 8 possible models. The saturated model contains five parameters and the remaining seven sub-models are constructed from different combinations of the presence or absence of three interaction parameters. Each model represents a different biologically plausible hypothesis, and hence has a different parameter set. Table 1 illustrates the parameterization of each model.

4.2. Edge correction

Since the observation window represents only a small subarea of the area of interest, interactions of plants outside the window with those inside the window cannot be directly considered. For example, if the unobserved points are close neighbours of an observed point, the number of close points (important consideration in secondary point pattern characteristics and

Table 1: Model notation – the presence or absence of a parameter from the full parameter set $\boldsymbol{\theta} = \{\kappa_1, \kappa_2, \eta_{11}, \eta_{22}, \eta_{12}\}$, is denoted by 1 or 0 respectively.

Model	Notation	Parameters present in model
1	10000	κ_1, κ_2
2	11100	$\kappa_1, \kappa_2, \eta_{11}$
3	11010	$\kappa_1, \kappa_2, \eta_{22}$
4	11110	$\kappa_1, \kappa_2, \eta_{11}, \eta_{22}$
5	11001	$\kappa_1, \kappa_2, \eta_{12}$
6	11101	$\kappa_1, \kappa_2, \eta_{11}, \eta_{12}$
7	11011	$\kappa_1, \kappa_2, \eta_{22}, \eta_{12}$
8	11111	$\kappa_1, \kappa_2, \eta_{11}, \eta_{22}, \eta_{12}$

in both pairwise and area interaction point processes) would be underestimated. We apply border (reduced sample estimator) edge correction (Baddeley and Turner 2000; Ripley 1988) to the data set (bivariate point pattern) and conduct a separate analysis on the reduced sample (bivariate point pattern after edge correction) to compare estimates of each interaction parameter. Models 2,3, and 5 are considered since these models contain only one interaction parameter; model 2 contains η_{11}, model 3, η_{22}, and model 5, η_{12} For this scenario, essentially, a border (the size of the interaction radius) is drawn 25 dm from the study border and points which fall on or outside of this border contribute to the pseudolikelihood only as neighbouring points to points within the reduced sample area. Other methods of edge correction include translation, reflection and torroidal edge correction. Importantly, (Pommerening and Stoyan 2006) note that some edge correction approaches may introduce more error/bias than if no edge correction method was applied. These authors suggest that the use of the reflection method for example, introduces a high level of bias. Conducting studies over large areas (plant communities in our case) is ideal for minimizing the edge effect.

We then compare the parameter estimates and model discrimination results obtained under both the scenarios of edge correction and no edge correction. The reduced sample is illustrated in Figure 7. There are approximately three clusters of points containing both species which fall outside the reduced sample.

4.3. Bayesian inference

The analyses were conducted in a Bayesian framework, and accordingly, priors for each parameter (including the models considered) were specified. A Uniform prior was specified for the intensity parameters where $\kappa \sim U[0, 1]$ and for the interaction parameters, a log normal prior was specified such that $\log(\eta) \sim N(0, \sigma^2)$, and $\sigma \sim U[0, 10]$. A prior sensitivity test was incorporated in our analyses to determine the dependence of the prior specification for the variance parameter on the results. As such, the following additional priors were considered: $\sigma \sim U[0, 1]$, $\sigma \sim U[0, 100]$.

For a fixed model we specify the pseudo-posterior distribution of the parameters in the form: $\pi(\boldsymbol{\theta}|\boldsymbol{x}) \propto PL(\boldsymbol{\theta}; \boldsymbol{x})p(\boldsymbol{\theta})$ where $p(\boldsymbol{\theta})$ denotes the (independent) priors specified on the parame-

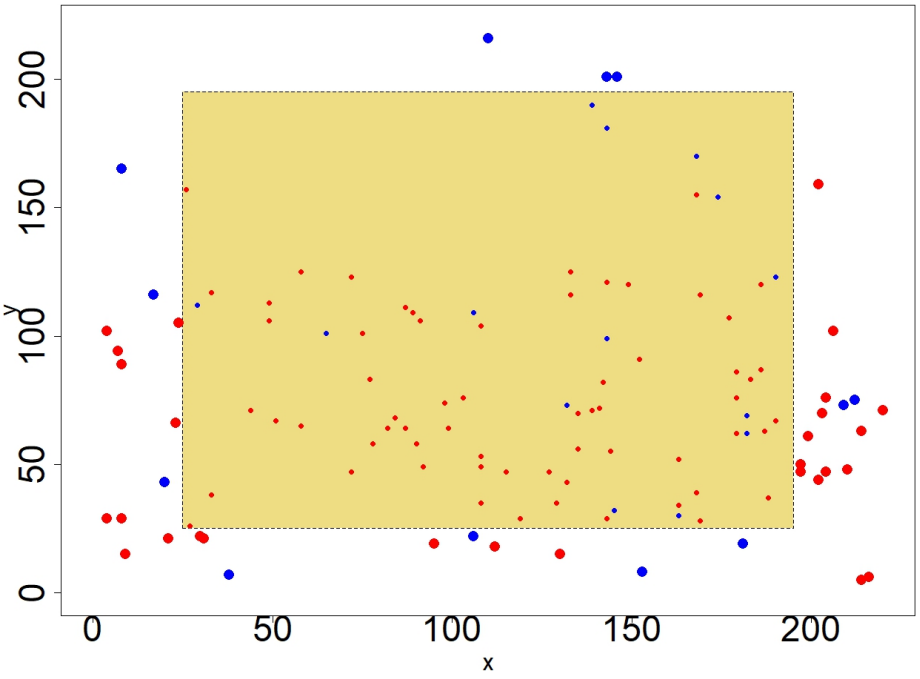

Figure 7: Plot showing the bivariate point pattern for the species pair comprising of *Astroloma xerophyllum* and *Banksia menziesii*. *Astroloma xerophyllum* is denoted by red filled circles. The reduced sample is the shaded area on the plot. The points which fall on or outside the border (illustrated in a dashed line) are the 'edge points'.

ters and $PL(\boldsymbol{\theta};\boldsymbol{x})$ the pseudo-likelihood given in equation 6. The constant of proportionality in the pseudo-posterior distribution is analytically intractable and equal to $[PL(\boldsymbol{\theta};\boldsymbol{x})p(\boldsymbol{\theta})]^{-1}$. Thus in order to obtain inference on the parameters $\boldsymbol{\theta}$, we employ an MCMC algorithm in order to estimate the posterior summary statistics of interest, for example, posterior mean and credible intervals, for the pseudo-posterior distribution.

Eight competing models were considered, which represent distinct research hypotheses. These correspond to the inclusion/exclusion of each possible interaction. The models considered are shown in Table 1. Each model was given equal probability of being selected in the model discrimination routine. Therefore, for a given model ω, the probability of being selected is 1/8.

In the presence of model uncertainty we extend Bayes' Theorem and consider the model to be an unknown parameter to be estimated. We then form the joint posterior distribution over both the models and the parameters:

$$\pi(\boldsymbol{\theta}_\omega, \omega|\boldsymbol{x}) \propto PL(\boldsymbol{\theta}_\omega;\boldsymbol{x})p(\theta_\omega|\omega)p(\omega)$$

where $\boldsymbol{\theta}_\omega$ denotes the set of parameters in model ω.

A Metropolis-Hasting sampler is used for updating the parameters in each model and the Markov chain Monte Carlo (MCMC) simulations were run for 10000 iterations (with 10% removed as burn in) to obtain posterior estimates for the parameters of each model. Model discrimination was performed used a reversible jump Markov chain Monte Carlo (RJMCMC) algorithm. Note that for the RJMCMC algorithm, an additional parameter is introduced– the model is treated as a parameter. This results in one Markov chain exploring both parameter and model space simultaneously. The routine consists of two stages which are discussed in turn below.

Suppose that at iteration t, the Markov chain is in model ω with parameter vector $\boldsymbol{\theta}_\omega$ so that the current model state is denoted as $(\boldsymbol{\theta}_\omega, \omega)$. The parameters are first updated given the current model state using an MCMC sampler such as the Metropolis Hastings or Gibbs samplers. This is the first stage of the RJMCMC procedure. The second stage involves updating the model. Firstly, a proposal to move to a new model, $\omega^{'}$ is made where each alternative model is chosen with some specified probability. The probabilities of moving from model ω to model ω', and from model ω' to model ω, are expressed as $P(\omega^{'}|\omega)$ and $P(\omega|\omega^{'})$ respectively. For this analysis, $P(\omega^{'}|\omega)$ and $P(\omega|\omega^{'})$ are equal to 1/8. This means that each of the eight models is selected with equal probability. Given the proposed model, new parameter values, $\boldsymbol{\theta}^{\boldsymbol{'}}_{\omega'}$, are generated. We specify a deterministic function, $g(\boldsymbol{\theta}_\omega, \boldsymbol{u}) = (\boldsymbol{\theta}^{\boldsymbol{'}}_{\omega'}, \boldsymbol{u}^{\boldsymbol{'}})$, where g is a bijective function such that $\boldsymbol{u}$ and $\boldsymbol{u}^{\boldsymbol{'}}$ are random variables and $g^{-1}(\boldsymbol{\theta}^{\boldsymbol{'}}_{\omega'}, \boldsymbol{u}^{\boldsymbol{'}}) = (\boldsymbol{\theta}_\omega, u)$. . Note that $\boldsymbol{u} \sim q(\boldsymbol{u}|\boldsymbol{\theta})$ and $\boldsymbol{u}^{\boldsymbol{'}} \sim q^{'}(\boldsymbol{u}^{\boldsymbol{'}}|\boldsymbol{\theta}^{\boldsymbol{'}})$ where q and $q^{'}$ are proposal distribution functions.

The proposal function, $q(.)$ generates candidate parameter values which are used in the MCMC acceptance function. The proposal function differs per model since each model consists of a different parameter set. For example, for model eight (which contains five parameters), we use a multivariate Gaussian distribution, $N(\boldsymbol{\mu}, \sum)$, to generate the candidate parameter values. For this model a pilot run was made where a Uniform distribution was used to generate each parameter (this method is know as a 'Uniform random walk'). This is specified as $U(\varpi - \iota, \varpi + \iota)$, where ϖ denotes the current parameter value (representing the current state in the MCMC chain) and ι, a tuning parameter. The posterior summary statistics (mean, variance) for this pilot model were then used to construct the mean vector, $\boldsymbol{\mu}$, and

covariance matrix, $\sum$, of the proposal function. The multivariate Guassian distribution was used because it leads to faster MCMC convergence (especially when correlated parameters are involved).

The move from model ω to model ω' is accepted with probability $\min(1, A)$, such that

$$A = \frac{\pi(\boldsymbol{\theta}'_{\omega'}, \omega'|\boldsymbol{x})P(\omega|\omega')q'(\boldsymbol{u}'|\boldsymbol{\theta}')}{\pi(\boldsymbol{\theta}_{\omega}, \omega|\boldsymbol{x})P(\omega'|\omega)q(\boldsymbol{u}|\boldsymbol{\theta})} \left| \frac{\delta(\boldsymbol{\theta}'_{\omega'}, u')}{\delta(\boldsymbol{\theta}_{\omega}, u)} \right| \tag{8}$$

where the final term is a Jacobian term. We note that if g is the identity function, then the Jacobian is equal to 1 and the $\delta(.)$ expression represents a partial derivative of the bijective function $g(.)$. The RJMCMC algorithm is summarized in Algorithm 1.

Input: $\omega = \{1, ..., n_\omega\}$, set of plausible models
Input: $\boldsymbol{\theta_\omega}$, set of parameters in model ω
Input: random variables $\boldsymbol{u}$ and $\boldsymbol{u'}$ proposed by $q(\boldsymbol{u}|\boldsymbol{\theta}), q'(\boldsymbol{u}'|\boldsymbol{\theta}')$.
Input: $P(\omega'|\omega)$, the probability of moving from model ω to model ω'
Input: $A = \frac{\pi(\boldsymbol{\theta}'_{\omega'}, \omega'|\boldsymbol{x})P(\omega|\omega')q'(\boldsymbol{u}'|\boldsymbol{\theta}')}{\pi(\boldsymbol{\theta_\omega}, \omega|\boldsymbol{x})P(\omega'|\omega)q(\boldsymbol{u}|\boldsymbol{\theta})} \left| \frac{\delta(\boldsymbol{\theta}'_{\omega'}, u')}{\delta(\boldsymbol{\theta}_{\omega}, u)} \right|$
Input: $\alpha(\boldsymbol{\theta}_\omega, \boldsymbol{\theta}'_{\omega'}) = \min(1, A)$; `// acceptance functions`
Output: Markov chain which traverses parameter and model space simultaneously
denote the initial model state as $(\boldsymbol{\theta}_\omega, \omega)$
for $t \leftarrow 1, \ldots, T$ **do**
  Metropolis Hastings step: update parameter values, $\boldsymbol{\theta}_\omega$, given the model state ω
  propose new model, ω', with probability $P(\omega'|\omega)$
  generate new parameter values, $\boldsymbol{\theta}'_{\omega'}$, given the proposed model ω'
  $r \sim U(0, 1)$
  if $r \leq \alpha(\boldsymbol{\theta_\omega}, \boldsymbol{\theta}'_{\omega'})$; `// accept/reject step`
  then
    model state at iteration $t + 1$ is updated to proposed model state and corresponding parameters ;
    `//` $(\boldsymbol{\theta}_{\omega'}, \omega')$
  end
  else
    model state at iteration $t + 1$ is identical to current model state at iteration t ; `//` $(\boldsymbol{\theta}_\omega, \omega)$
  end
end

Algorithm 1: The reversible jump MCMC algorithm

4.4. Model assessment

The model was assessed by comparing 500 instances (simulated data from the model) to that observed. The cross pair correlation function for multitype point patterns was used to compare the simulated data to the observed data.

5. Results

5.1. Parameter estimates

The posterior estimates for the parameters are given in Table 2. We note that the mean posterior parameter estimates for the interactions obtained are consistent with the results obtained in the exploratory analysis. In particular, the estimated posterior mean (standard

deviation) for the log intraspecific interaction parameter in species 1 in model 2 (the model which contains only this interaction) is 4.00 (0.62), signifying attraction. The exploratory analysis indicated that the sub-pattern corresponding to this species was clustered. We note also that the posterior estimates for this parameter are consistently positive across all the models which contain it.

In model 3, the model which contains only one interaction parameter (which represents the log interaction between plants of species 2), the mean (standard deviation) posterior estimate is 0.59 (0.62); providing no evidence for an interaction among plants of species 2. The exploratory analysis indicated that the sub-pattern representing this species exhibited complete spatial randomness (CSR). Note that across all the models (which contain this interaction parameter), the credible intervals of the posterior estimate for the log interaction between individuals of species 2 all contain zero.

The relative strengths of the intraspecific and interspecific interactions appear to differ. For example, in the saturated model, consider the log intraspecific interaction in species 2. The mean posterior estimate is 0.75(0.44) whilst that for the log interspecific parameter is 5.19(0.36). Clearly the log interspecific interaction is one of attraction (the credible intervals across all models containing this parameter contain non negative values), whilst that of the intraspecific interaction parameter in species 2 appears to be negligible. We note that the posterior estimates for the log interspecific parameter are consistently positive across all the models which contain it.

	summary	model 1	model 2	model 3	model 4	model 5	model 6	model 7	model 8
κ_{11}	mean	0.001898	6.7e-05	0.001918	7.9e-05	0.000124	1e-05	0.000144	1.1e-05
	2.5%	0.001593	2e-05	0.001599	2.6e-05	8.4e-05	3e-06	7.9e-05	4e-06
	97.5%	0.002254	0.000142	0.002276	0.000171	0.000167	1e-05	0.000231	2e-05
κ_{22}	mean	0.000556	0.000553	0.000413	0.000381	3.6e-05	4.6e-05	2.9e-05	3e-05
	2.5%	0.000394	0.000426	0.000174	2e-04	2.3e-05	2.8e-05	1e-05	1.4e-05
	97.5%	0.000739	0.000686	0.000721	0.000595	5e-05	6.5e-05	6.2e-05	5.1e-05
η_{11}	mean		4.001075		3.828321		3.124417		2.983804
	2.5%		3.007814		2.835776		2.406887		2.127593
	97.5%		5.021521		4.77873		3.990988		3.938942
η_{22}	mean			0.590241	0.690396			0.701177	0.750893
	2.5%			-0.302122	-0.053537			-0.337348	0.033798
	97.5%			1.686791	1.436854			1.788376	1.472338
η_{12}	mean					5.578262	5.19695	5.37953	5.199629
	2.5%					5.07291	4.634955	4.540732	4.620373
	97.5%					6.11549	5.78256	6.191106	5.813661
σ	mean		5.36505	3.231871	5.725265	6.559747	6.215054	4.910265	5.445704
	2.5%		2.125722	0.226316	1.869868	2.899072	2.935592	2.284667	2.490686
	97.5%		9.19976	7.967917	14.987599	9.611484	9.502591	8.370077	9.0334

Table 2: Posterior means and 95% credible estimates for parameters (2.5% quantiles are provided).

A prior sensitivity analysis was conducted where $\sigma \sim U(0,1)$ and $U(0,100)$. We note that the interaction parameter values for the prior $\sigma \sim U(0,1)$ are slightly lower than that obtained with the other priors, indicating a degree of prior sensitivity. This is because this parameter,

Table 3: Model posterior probabilities for prior sensitivity analysis ($\sigma \sim U(0, 10)$, $\sigma \sim U(0, 1)$, and $\sigma \sim U(0, 100)$).

Model	$U[0, 10]$	$U[0, 1]$	$U[0, 100]$
1	0.026	0.018	0.027
2	0.021	0.016	0.021
3	0.021	0.015	0.015
4	0.020	0.011	0.022
5	0.101	0.151	0.142
6	0.345	0.515	0.349
7	0.139	0.063	0.105
8	0.326	0.211	0.318

σ, is constrained under the prior $\sigma \sim U(0, 1)$.

5.2. Model discrimination and assessment

For this data set, there are 8 competing models $\omega = \{1, ..., 8\}$ (see Table 1 for the model indicators). The eight models considered in this analysis can be formally compared by using model discrimination methods. In particular, model posterior probabilities are obtained, providing a quantitative comparison of the models. An RJMCMC algorithm was implemented for this purpose.

Table 3 shows the posterior model probabilities obtained for the analysis where $\sigma \sim U(0, 10)$ and for the additional priors used in the prior sensitivity analysis. From this table, it is observed that the model which received the highest posterior support is model 6, the model with the interspecific interaction parameter and the intraspecific interaction parameter for species 1. Lindley's paradox is observed in this analysis – as the variance of the prior is increased ($\sigma \sim U[0, 100]$), the models with fewer parameters (models 1 to 4 in particular) obtained an increase in posterior support.

From Table 3, it is observed that the posterior probability of the interspecific parameter η_{12} being present in a model is 91.13. The probabilities for the other interaction parameters η_{11} and η_{22} are 7.12 and 5.07 respectively, which are clearly much lower than that for η_{12}. We note that the model identified with the highest posterior support contains both η_{11} and η_{12}.

Finally, model 6 was assessed by comparing simulated data from the model using a move-birth-death algorithm based on that proposed by Møller and Waagepetersen (2003) to the observed data. The cross pair correlation function for the simulated data was compared to that obtained for the observed data as done by Picard *et al.* (2009). Overall the cross pair correlation function for the simulated data (see Figure 8(a)) is consistent with that for the observed data at most distances. In both cases clustering between the two species involved is observed at the interpoint distance (r) of 25dm. Figure 8(b) shows an example of a simulated data set. In this plot there is evidence of clustering together of points representing both species and also a concentration of points at one side of the plot - similar to that observed in the observed data in Figure 2.

Differences in the cross K_{12} function for these data sets may have been caused by unob-

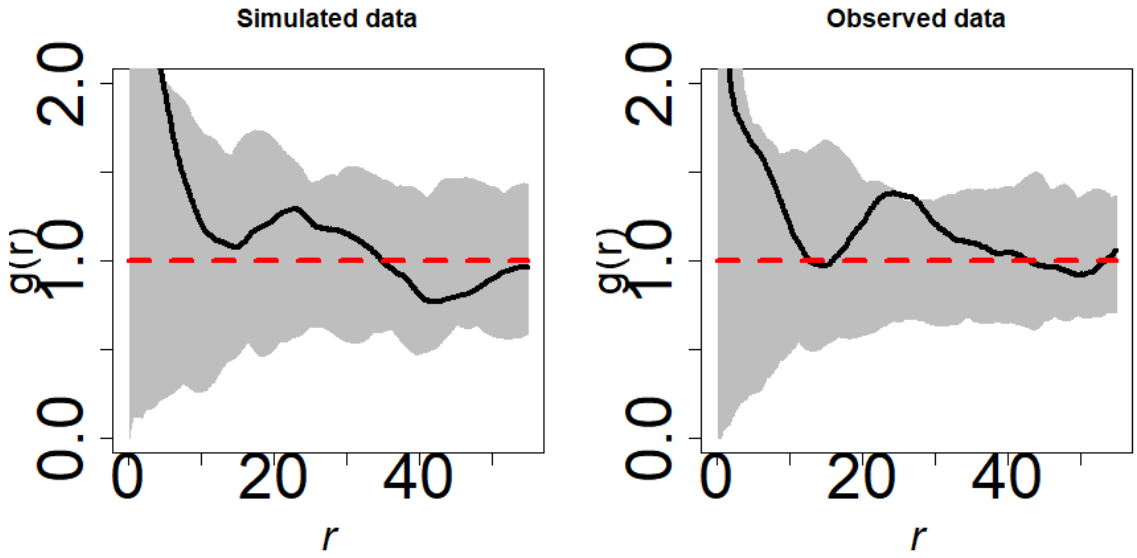

(a)

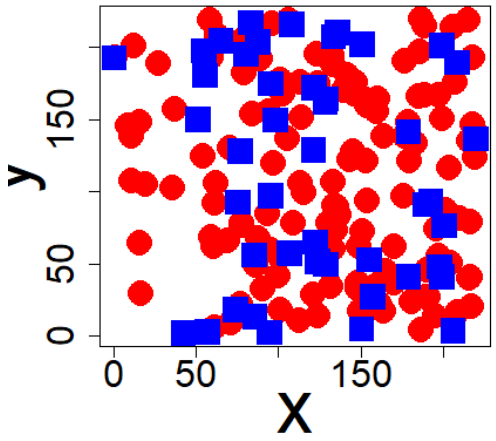

(b)

Figure 8: Plots showing (a) the cross K_{12} function for the observed data (blue line),700 simulated point patterns (grey lines), and the Poisson reference (red line), and (b) an example of a simulated bivariate point pattern (species 2 is denoted by blue squares).

served environmental factors and a resulting inhomogeneity, as observed for species 1 in the exploratory analysis and to the fact that the interspecific interactions are assumed to be symmetric - that is the effect of species 1 on species 2 is assumed to identical to the reverse. Future work will introduce asymmetric interspecific interactions into the modelling approach.

5.3. Edge Correction

After border edge correction was applied, the number of points in the resulting bivariate point pattern was reduced from 117 to 77; the edge points were mostly clusters containing individuals of mostly species 1 and lone points of species 2. Specifically, the number of points for species two was decreased to 54% of the original sample size, whilst that for species 1 was reduced to 69% of the original sample size. The reduction in points led to smaller posterior parameter estimates for the intraspecific interaction parameters and a larger posterior estimate for the interspecific interaction parameter. For example, the intraspecific interaction parameter for species 1 was estimated as 4.00 (3.01, 5.02) before edge correction; after edge correction, the said parameter was estimated as 2.55 (1.73,3.46). The overall inference, however, that there is an interaction amongst tress of this species of attraction remains.

6. Discussion

From the results, we note that the use of the area interaction process facilitated the identification of both inhibitory and attractive interactions. The interspecific interaction is found to be attractive. The flexibility of an area interaction process to model both inhibitory and attractive interactions makes it suitable for modelling data sets which possess a range of interactions which might posses attractive as well as repulsive interactions.

The results also indicate that there is very strong support for the presence of the interspecific parameter, an indication of decisive posterior support for this parameter. In addition, the model with the highest posterior support is model 6 which contained two interaction parameters; the intraspecific interaction parameter for *Astroloma xerophyllum* and the interspecific interaction parameter between the two species. A possible explanation for the attraction between the two species is that the *Astroloma xerophyllum* species benefits from being in close proximity to the extensive proteoid roots of the Banksia species which modify the surrounding soil conditions facilitating nutrient uptake. In addition, *Astroloma xerophyllum* has been reported to exist in symbiotic associations or mycorrhizas with ericoidal fungi (Bell and Pate 1996; Read 1995). The clustering of individuals of this species may be due to associations between more than one *Astroloma xerophyllum* plant with the same ericoidal fungus, the presence of which improves the efficiency of nutrient uptake by the associated plant. Studies aimed at modelling the spatial positions of ericoidal fungi and *Astroloma xerophyllum* would help clarify these clustered patterns. These symbiotic associations were not identified in the univariate exploratory analyses - thus demonstrating the limited insight provided due to only considering partial information.

The differences observed between the analyses with and without edge correction suggest that the particular edge correction approach adopted for a given analysis may affect the results significantly. In addition, it is evident that the decision to apply edge correction (and the choice of edge correction) should be informed by other information such as the representativeness of the study area and the underlying environmental conditions in the study area. If the en-

vironmental conditions are heterogenous for example, the intensity of points representing the individuals concerned would not be constant throughout the study area. This would create a case for edge correction since it is more difficult to sample a representative plant community from a region that is heterogenous in terms of plant density and environmental conditions.

Further analyses aimed at investigating the nature of the interspecific interactions (whether or not they are asymmetric) would shed light on the underlying factors which give rise to the spatial distribution of the two species. This would necessitate the use of an asymmetric point processes. In this paper we have assumed that the interaction between the species is symmetric – that is the effect of one species is identical to the reciprocal interaction. As a result we have used the same interaction radius for both species. An extension to this approach would be to adopt an asymmetric area interaction point process to model data sets without the assumption that the interspecific interactions are symmetric. In this case the interaction radii for the two species may be specified differently.

The quantification of inter- and intraspecific interactions is especially valuable for preserving biodiversity and for informing reforestation and land rehabilitation efforts after wildfires.

References

Atwell BJ, Kriedemann PE, Turnbull CG (1999). *Plants In Action*. Macmillan Education Australia Pty Ltd.

Baddeley A, Lieshout M (1995). "Area Interaction Point Processes." *Annals of the Institute of Statistical Mathematics*, **47**, 601–619.

Baddeley A, Turner R (2000). "Practical Maximum Pseudolikelihood for Spatial Point Patterns." *Australian and New Zealand Journal of Statistics*, **42**, 283–322.

Bell DT (2001). "Ecological Response Syndrome in the Flora of Southwestern Western Australia: Fire Resprouters versus Reseeders." *The Botanical Review*, **67**.

Bell TL, Ojeda F (1999). "Underground Starch Storage in Erica species of the Cape Floristic Region Ű Differences Between Seeders and Resprouters." *New Phytologist*, **144**.

Bell TL, Pate JS (1996). "Nitrogen and Phosphorus Nutrition in Mycorrhizal Epacridaceae of South West Australia." *Annals of Botany*, **77**, 389–397.

Casper BB, Schenk HJ, Jackson RB (2003). "Defining a Plant's Belowground Zone of Influence." *Ecology*, **84**(9), 2313–2321.

Illian J, Møller J, Waagepetersen RP (2009). "Hierarchical Spatial Point Process Analysis for a Plant Community with High Biodiversity." *Environmental and Ecological Statistics*, **42**, 283–322.

Illian JB, Hendrichsen DK (2010). "Gibbs Point Process Models with Mixed Effects." *Environmetrics*, **21**, 241 – 353.

King R, Illian JB, King SE, Nightingale GF, Hendrichsen DK (2012). "A Bayesian Approach to Fitting Gibbs Processes with Temporal Random Effects." *Journal of Agricultural, Biological, and Environmental Statistics*, **17**, 601–622.

Kruger LM, Midgley JJ, Cowling RM (1997). "Resprouters vs Reseeders in South African Forest Trees; a model based on forest canopy height." *Functional Ecology*, **11**.

Levine JM (2000). "Complex Interactions in a Streamside Plant Community." *Ecology*, **81**, 3431–3444.

Møller J, Waagepetersen RP (2003). *Statistical Inference and Simulation for Spatial Point Processes*. Chapman and Hall/CRC.

Nightingale GF, Illian JB, King R (2015). "Pairwise Interaction Point Processes for Modelling Bivariate Spatial Point Patterns in the Presence of Interaction Uncertainty." *Journal of Environmental Statistics*, **7**.

Picard N, Bar-Hen A, Mortier F, Chadœuf J (2009). "The Multi Scale Marked Area Interaction Point Processes: A Model for the Spatial Pattern of Trees." *Scandinavian Journal of Statistics*, **36**, 23–41.

Pommerening A, Stoyan D (2006). "Edge-correction needs in estimating indices of spatial forest structure." *Canadian Journal of Forest Research*, **36**, 1723–1739.

Read DJ (1995). "The Structure and Function of the Ericoid Mycorrhizal Root." *Annals of Botany*, **77**, 365–374.

Ripley BD (1988). *Statistical inference for spatial processes*. Cambridge University Press.

Stoyan D, Stoyan H (1996). "Estimating Pair Correlation Functions of Planar Cluster Processes." *Biometrical Journal*, **38**, 259–271.

Tedersoo L (2017). *The Biogeography of Mycorrhizal Symbiosis*. Springer.

Turnbull LA, Levine JM, Loreau M, Hector A (2013). "Coexistence, Niches and Biodiversity Effects on Ecosystem Functioning." *Ecology Letters*, **16**, 116–127.

van Lieshout MNM (2000). *Markov Point Processes and their Applications*. Imperial College Press, London, UK.

van Lieshout MNM (2006). "Markovianity in Space and Time." *Lecture Notes Monograph Series Dynamics and Stochastics*, **48**, 154–168.

Affiliation:

Glenna Nightingale
University of Edinburgh
School of Health in Social Science, Edinburgh, U.K
E-mail: glenna.evans@gmail.com
URL: http://www.glenna.nightingale.com/

Journal of Environmental Statistics http://www.jenvstat.org
Volume 09, Issue 2 Submitted: 2017-08-17
September 2019 Accepted: 2019-09-19